Title
Chemical and Structural Evolution of AgCu Catalysts in Electrochemical CO2 Reduction

Journal
Journal of the American Chemical Society, 145(18)

ISSN
0002-7863

Authors
Chen, Peng-Cheng
Chen, Chubai
Yang, Yao
et al.

Publication Date
2023-05-10

DOI
10.1021/jacs.3c00467

Peer reviewed

The chemical and structural fate of AgCu catalysts in electrochemical CO_2RR

Peng-Cheng Chen[1,2,†], Chubai Chen[2,†], Yao Yang[2,3,†], Arifin Maulana[4], Jianbo Jin[2], Julian Feijoo[2], Peidong Yang[1,2,4*]

[1]Kavli Energy Nanoscience Institute, [2]Department of Chemistry, [3]Miller Institute, [4]Department of Materials Science and Engineering, University of California, Berkeley, California 94720, United States.

*Corresponding author. Email: p_yang@berkeley.edu

†These authors contributed equally to this work.

Abstract:

Silver-copper (AgCu) bimetallic catalysts hold great potential for electrochemical carbon dioxide reduction reaction (CO_2RR), which is a promising way to realize the carbon neutrality goal. Although a wide variety of AgCu catalysts have been developed so far, it is indeed underexplored how AgCu catalysts evolve during the reaction. The absence of insights into their stability makes the catalytic sites elusive and hampers the design of effective AgCu catalysts in a rational manner. Here, we synthesized phase-blended and phase-separated AgCu nanoparticles on carbon paper electrodes and investigated their evolution behavior in CO_2RR. Our time-sequential scanning transmission electron microscopy and elemental mapping studies show that Cu possesses high mobility under the reaction conditions, which can leach out from the catalysts by migrating to the catalyst surface, detaching from the catalysts, and agglomerating as new particles. Moreover, Ag and Cu manifest a trend to phase-separate into Cu-rich and Ag-rich grains, regardless of the starting catalyst structure. The composition of the Cu-rich and Ag-rich grains diverge during the reaction and eventually approach thermodynamic values, *i.e.*, $Ag_{0.88}Cu_{0.12}$ and $Ag_{0.05}Cu_{0.95}$. The separation between Ag and Cu has been observed in the bulk as well as on the surface of the catalysts, highlighting the importance of Ag-Cu phase boundaries for CO_2RR. In addition, *operando* X-ray absorption spectroscopy study was applied to confirm the zero-valence state of Cu as the catalytically active sites during the electrolysis process. Taken together, this work provides a comprehensive understanding of the chemical and structural evolution of AgCu catalysts during the CO_2RR.

Main Text:

Electrochemical carbon dioxide reduction reaction (CO_2RR), with the capability of utilizing CO_2 as a feedstock to generate value-added chemicals, has the promise to lessen the dependence on fossil fuels and decouple CO_2 emissions from economic growth, thus attracting broad interest in recent years.[1-6] Thus far, Cu is the only monometallic catalyst that can effectively convert CO_2 to multicarbon products, which becomes the most important catalytic system for electrochemical CO_2RR. However, the Cu system alone is not ideal for transforming CO_2 to CO and thereby limits the subsequent generation of multicarbon products.[6-8] One strategy to improve the CO_2RR performance of Cu is to construct a multimetallic system, where Cu and the other metal components can function synergistically.[9-12] For example, Ag is a promising candidate metal to be incorporated into the catalytic system because of its high efficiency of generating CO from CO_2,[13,14] and its thermodynamic immiscibility with Cu.[15-18] In view of its potential, many efforts have been put on developing AgCu bimetallic catalysts for CO_2RR.

Based on the interaction between Cu and Ag, AgCu bimetallic catalysts can be classified into three categories. In the first group, Ag and Cu are physically mixed to form tandem catalysts where Ag creates a CO-concentrated local environment that can be utilized by Cu to boost the generation rate of multicarbon products.[19-22] Inspired by this design principle, in the second category, AgCu nanostructures that are rich in phase boundaries between Cu and Ag have been devised to further enhance the spillover of CO from the Ag sites to the Cu surface.[23-28] Lastly, even though Cu and Ag are highly immiscible metals, the mixing energy change caused by the large surface area of nanostructures makes the alloying between Cu and Ag possible at the nanoscale.[29] Therefore, multiple strategies have been established to introduce Ag atoms into Cu phase, such as galvanic replacement,[30,31] co-sputtering,[32] ligands assisted co-deposition,[33] oxidation/reduction-driven atomic interdiffusion,[34] and thermal shocking synthesis.[35] Although a wide range of AgCu catalysts have been successfully made for CO_2RR, surprisingly, the chemical and structural evolution of AgCu is barely investigated despite the fact that catalysts are often unstable under the electrochemical environment.[36-39] Considering the rich chemistry of Cu and Ag at the nanoscale that will principally make the further optimization of AgCu catalysts feasible, understanding the chemical and structural fate of AgCu electrocatalysts will be crucial

for the design of novel AgCu and other multimetallic catalysts with superior activity and stability.

Herein, we synthesized two types of AgCu catalysts, *i.e.*, alloyed and phase-separated AgCu particles, and systematically explored their evolution behavior in CO_2RR. We found that the two types of catalysts evolve into similar structures primarily due to the high mobility of Cu under the CO_2RR conditions (Figure 1). For AgCu alloy catalysts, Cu will leach out from the catalysts during CO_2RR, which is subsequently enriched on the particle surface or recrystallized elsewhere as new particles. For phase-separated AgCu catalysts, the Cu domains are corroded during CO_2RR and migrate to the Ag domain surface, resulting in structures similar to what has been observed in the AgCu alloy case. While Ag and Cu generally tend to phase separate as the reaction proceeds owing to their high immiscibility, the two elements are still slightly mixable to form Ag-rich and Cu-rich domains in the nanocatalysts within the thermodynamic solubility limit.

The AgCu alloy nanoparticles were prepared by microwave-assisted shock synthesis. Experimentally, carbon paper substrates loaded with Ag and Cu salt precursors were first irradiated by microwave to instantly raise the temperature to higher than 1000 ˚C.[40] This high temperature will thermally decompose the salt precursors while allowing Ag and Cu to be mixed in a liquid state (Figure S1). The elemental mixture was then quenched by rapid cooling when the irradiation was off to yield the AgCu alloy particles. As shown in Figure 2A and S2, AgCu nanoparticles with size between 10-100 nm were successfully synthesized via this method. Energy dispersive X-ray spectroscopy (EDS) analysis confirms that the nanoparticles have an average composition of $Ag_{0.5}Cu_{0.5}$, and the two elements are uniformly distributed in the nanoparticles. Notably, magnified EDS mapping of individual nanoparticles reveals that the particles are indeed composed of Cu-rich and Ag-rich grains of size smaller than 10 nm (Figure S3), rather than forming single-phase AgCu mixture. The co-existence of Ag-rich and Cu-rich phases was further corroborated by X-ray diffraction (XRD) characterization (Figure 2B), which exhibits two sets of diffraction peaks that can be assigned to the two phases, respectively. Importantly, the diffraction peaks were found to slightly shift when compared with the standard peaks of monometallic Cu and Ag, suggesting that the two phases are not compositionally pure. Ag and Cu are inter-doped in these Ag-rich and Cu-rich grains. Further, high-resolution transmission electron microscopy (HRTEM) characterization was carried out to gain more

insights into the particle structure at an individual particle level. As shown in Figure 2C and S4, the AgCu nanoparticles have an fcc lattice structure. Fast Fourier transform (FFT) of selected area confirms the presence of Ag-rich and Cu-rich lattices. In some particles, the two types of grains are coherently oriented and moiré patterns with a 1.82 nm spacing can be observed due to the periodical lattice matching between the Ag (111) and Cu (111) planes. In addition, a ~2 nm thin-oxide layer can be found on the nanoparticle surface, likely caused by Cu oxidation upon exposing the particle to air. Collectively, these characterizations confirm that the as-synthesized $Ag_{0.5}Cu_{0.5}$ nanoparticles consist of a mixture of Ag-rich and Cu-rich grains (< 10 nm), *i.e.*, a phase-blended structure. For simplicity, we name this AgCu phase-blended structure as AgCu alloy in the following text.

Electrochemical CO_2RR was performed on the as-synthesized AgCu alloy nanoparticles in 0.1 M $KHCO_3$ electrolyte using a three-electrode system in conventional H-cells. Considering that the evolution behavior of monometallic Cu under CO_2RR has been reported to strongly relate to the applied potential as well as the binding intermediates,[37-39,41-43] we chose a moderate potential (-1.0 V vs. RHE) as a representative condition to conduct the CO_2RR. Under this reaction potential, the faraday efficiency (FE) towards hydrogen evolution reaction (HER) and CO_2RR is roughly equal (Figure S4). High-angle annular dark-field scanning transmission electron microscopy (HAADF-STEM) and EDS characterizations were performed on the AgCu catalysts that have catalyzed CO_2RR for a specific time between 0-24 h. As shown in Figure 3a, Cu and Ag exhibit a trend to separate from each other during the reaction. After 0.5 h of electrolysis, enrichment of Cu species on the catalyst surface can already be observed (Figure 3a, second column). When the electrolysis time is extended to 1 h or 3 h, more Cu species are leached out and migrate to the catalyst surface, leading to a thicker layer of Cu on the particles (Figure 3a, third to fourth column). Meanwhile, some Cu particles (< 5 nm) are detached from the parental AgCu catalysts (Figure S5). When the reaction time is further prolonged to 6 h, individual Cu particles with size > 10 nm and are not in proximity to the original AgCu particles can be observed (Figure 3a, fifth column), which is presumably formed by coalescence of the detached Cu particles. After 24 h of electrolysis, Cu is severely segregated from Ag, either forming large-size grains that still stick to the original particles or agglomerating elsewhere as new particles (Figure 3a, last column, and Figure S7). The structural evolution of the AgCu alloy catalysts is also reflected in their XRD patterns (Figure 3b). It can be seen that the (111) peak

assigned to the Cu-rich grains is flattened when the reaction starts, due to the reduced crystallinity of Cu when it degrades from the catalysts. Moreover, the (111) peak belonging to the Ag-rich grains gradually shifts to lower-angle positions after the electrolysis, suggesting the leaching of the Cu dopants from the Ag-rich grains during the reaction process. However, even after 24 h of electrolysis, the (111) peak position of Ag-rich grains is higher than that of standard Ag, indicating that there is still a certain amount of Cu doped in the Ag-rich grains. Ex-situ HRTEM characterization further supports the structural evolution behavior of the catalysts (Figure 3c and S6). Before the electrolysis, a 2-nm air-induced Cu_2O layer can be observed through HRTEM. After 3 h of reaction, larger Cu_2O grains (2-8 nm) were developed on the catalyst surface. Further extending the electrolysis time results in larger-size Cu domains that are observable under HRTEM. It should be noted although we observe Cu_2O lattices in the catalysts that were taken out from the reaction, these oxides are formed because of the air exposure after electrolysis. Our *operando* X-ray absorption spectroscopy (XAS) study in the following text has proven that the Cu species maintain a metallic state under the reaction environment. Compared with the poor stability of Cu in CO_2RR, Ag is much less mobile in CO_2RR, as evidenced by the minor change of the Ag-containing particle size (Figure S8). Taken together, it is clear that the Cu and Ag in the AgCu mixed particles will structurally separate with each other during CO_2RR. Cu species migrate to the catalyst surface and grow into large-size grains, or detach from the catalyst surface and agglomerate as new particles.

To further elucidate the separation state between Ag and Cu during CO_2RR, in particular whether the two elements have been completely de-alloyed as suggested by the phase diagram, we conducted a compositional analysis on the Ag-rich and Cu-rich phases using a combination of XRD, selected area electron diffraction (SAED), and EDS (Figure 4). For the Ag-rich phases, the d-spacing of (111) planes is gradually increased when the electrolysis proceeds but it remains smaller than that of pure Ag, as evidenced by both XRD characterization of the catalyst ensemble and SAED analysis of selected nanoparticles (Figure 4b, 4c, and S9). The results confirm the leach-out of Cu from the original Ag-rich phase until a new stable Ag-rich phase with a lower Cu content is established. EDS analysis was utilized to quantify the composition of the entire particle catalyst, the Ag-rich domain, and the leached Cu domain. As shown in Figure 4d, 4e, and S10, the Cu content in the Ag-rich domain decreases until a steady state containing ~12% of Cu is achieved after ~3 h of electrolysis. This specific composition, $Ag_{0.88}Cu_{0.12}$, can be

considered as the thermodynamically stable composition of the Ag-rich phase under CO_2RR conditions. Within a similar reaction time, the Cu content of the leached Cu domain increases to ~95%. Therefore, Ag and Cu are not fully separated from each other in CO_2RR. The original AgCu alloy is converted from a metastable state to thermodynamically stable Ag-rich and Cu-rich phases that can be denoted as $Ag_{0.88}Cu_{0.12}$ and $Ag_{0.05}Cu_{0.95}$, respectively. In the meantime, we found that the Cu content of the entire particle catalysts is continuously decreased during the electrolysis. Given the low solubility of Cu in the electrolyte (0.1 M $KHCO_3$),[38,45] the decreased Cu content cannot be explained by the dissolution of Cu into the electrolyte. We hypothesize that this part of Cu migrates from the catalyst surface to the carbon substrate during the electrolysis, which then agglomerates to form those isolated Cu-rich particles (Figure 3a and S7).

To further verify whether the two unique phases we observed in the AgCu catalysts, *i.e.*, $Ag_{0.88}Cu_{0.12}$ and $Ag_{0.05}Cu_{0.95}$, are thermodynamic products, we utilized thermal treatment to transform AgCu alloy catalysts into phase-separated structures, which are supposed to be thermodynamically stable (Figure 5 and S11). Notably, the composition of Cu and Ag domains in the phase-separated nanoparticles is found to be close to what we observed in the AgCu alloy catalysts after 3 h of CO_2RR. When these phase-separated AgCu catalysts were applied for 3 h of CO_2RR, the Cu domains in the phase-separated AgCu particles are corroded and migrated to the Ag domain surface, resulting in structures similar to the AgCu alloy case (Figure 5a and S12). Moreover, the composition of Ag and Cu domains measured by EDS remains unchanged after the electrolysis (Figure 5b and S11). Besides, there is a negligible peak shift of the Ag (111) and Cu (111) planes in the XRD patterns of catalysts before and after electrolysis (Figure 5c). As such, we conclude that $Ag_{0.88}Cu_{0.12}$ and $Ag_{0.05}Cu_{0.95}$ are thermodynamic phases in AgCu nanoparticles, which are also stable under the CO_2RR environment.

The structural and compositional studies of the alloyed and phase-separated AgCu nanoparticles clearly point out the separation of Ag and Cu in catalysts during CO_2RR. Since electrocatalysis indeed happens on catalyst-electrolyte interface, surface structure rather than bulk dictates the catalytic results, of which the importance cannot be ignored. Recently, many technologies have been built up to advance our understanding of surface chemistry in electrocatalysis.[46,47] Among the various surface characterization technologies, electrochemical methods exhibit their unique advantage by directly acting on the electrode surface and therefore are sensitive to the local chemical environment. For example, H-underpotential deposition has

become a classic method to probe the surface area and active sites of Pt-based catalyst[48] and the redox peak of Ir can be a method to quantify the Ir sites in oxygen evolution catalysts.[36] However, the electrochemical characterization of Cu surfaces is more challenging for various reasons. Although double-layer capacitance can be used to quantify the electrochemical surface area (ECSA) of Cu foil or mesh, it is not applicable for the carbon-supported Cu nanoparticles due to the large capacitance contributed from the substrates. Meanwhile, the dynamic nature of Cu atoms during the redox cycles often makes surface characterization ambiguous, because of the possible severe surface and even bulk structural change. In view of this, researchers have used OH^- adsorption peak to identify the Cu surface structure[49] but these characteristic peaks are also partially overlapped with the Cu oxidation peak, making it challenging to determine the sweeping potential window and to analyze the corresponding results.

Recently, Pb underpotential deposition (Pb-UPD) has been utilized to characterize Cu surface, which is sensitive to the surface structure and has a high signal-to-noise ratio since there is no contribution from the carbon substrates.[50,51] Therefore, we investigated the surface structure of AgCu catalysts with this method (Figure 6 and S13). Commercial Cu and Ag foil were utilized as references, which exhibits Pb stripping peaks at -0.254 V and -0.284 V vs. Ag/AgCl (3M KCl), respectively (Figure 6a). Interestingly, in stark difference from the reference, a major stripping peak located at -0.303 V and a tiny stripping peak located at -0.226 V can be found in the first CV cycle of the AgCu alloy particles, which may be attributed to the Pb stripping from the alloy phases and the defected Cu sites,[50] respectively. The minor peak belonging to the defected Cu (-0.226 V) becomes larger in the initial few CV cycles and then vanishes, which can be correlated to Cu leaching, migration, and aggregation. In addition, unlike the Cu and Ag foil, which is stable under the Pb-UPD condition, the Pb stripping peaks of the AgCu alloy particles evolve quickly (Figure 6c). It can be seen that the pristine -0.303 V peak gradually decreases and separates into two peaks that match well with the peak positions of the Cu and Ag foil. This indicates that during the electrochemical CO_2RR, the surface of the AgCu alloy also experiences phase-separation, resulting in Cu- and Ag-dominated phases. Since the Pb stripping peak only reflects the binding strength between the metal surface and Pb atoms, it is arguable whether the surface comprises of pure Cu and Ag phases, or the trace inter-doping of metals does not significantly influence the Pb-binding affinity. However, considering that the inter-doped phases in the heterostructured AgCu particles exhibit a shift of Pb-stripping peaks (Figure 6b), we

believe there is no inter-doping between Cu and Ag on the particle surface after the phase-separation caused by CO_2RR. Collectively, our Pb-UPD experiments confirm that AgCu mixture is not stable under CO_2RR conditions. Not only the bulk, but also the surface of AgCu catalysts goes through an electrochemically triggered phase-separation. The results also imply that the enhanced CO_2RR performance reported on AgCu catalysts[19-28,30-34] could be originated from AgCu heterostructures. Such structures can promote CO_2RR tandem catalysis between the Ag and Cu domains, as well as boost CO_2RR via the asymmetric coupling sites that are rich around the AgCu interface. Therefore, constructing phase boundary-rich AgCu catalysts will be beneficial for enhanced CO_2RR.

Besides investigating the structural fate of AgCu catalysts, we further employed *operando* high-energy resolution fluorescence detector (HERFD) X-ray absorption spectroscopy (XAS) to unravel the chemical fate of the catalysts during CO_2RR, *i.e.*, the electronic structure and coordination environment of AgCu alloy electrocatalysts under real-time reaction conditions. The HERFD detector selects Cu $K\alpha_1$ emission line as one particular fluorescence decay channel, which significantly extends the core hole lifetime.[52,53] Thus, the HERFD XAS can allow a much higher energy resolution on the order of 1 eV, given the energy-time uncertainty principle, when compared to a conventional X-ray fluorescence detector (50-200 eV).[54-56] HERFD X-ray absorption near-edge structure (XANES) spectroscopy resolves the pre-edge peaks of Cu, Cu_2O, and CuO reference samples, which are significantly better than conventional XANES spectra, as exemplified by the notable identification of pre-peak of CuO at ~8977 eV originating from the Jahn-Teller distortion of $[Ar]3d^9$ configuration (Figure S14). Cu_2O shows the characteristic pre-edge peak at 8981.0 eV with a 1.2 eV positive shift, relative to Cu (8979.8 eV). The home-made HERFD XAS electrochemical cell[57] is capable to deliver electrochemical results of AgCu alloy electrocatalysts comparable to a standard H-cell with a well-defined current plateau under the CO_2RR condition (Figure S15).

Operando XANES of AgCu alloy electrocatalysts were performed during the CO_2RR (Figure 7a). XANES spectrum of pristine AgCu alloys presents the co-existence of metallic Cu and Cu_2O, when compared to standard references (Figure 7b, dashed lines). At -1.0 V vs. RHE, XANES pre-edge peaks at ~8979 eV show progressive negative shifts, particularly after 40 min, corresponding to the electroreduction of Cu_2O to metallic Cu. In addition, post-edge peaks at 9002.5 and 9024 eV (dashed red arrows in Figure 7a) further support the conversion of Cu_2O to

Cu under the reaction environment (Figure S14b). Quantitative analysis using pre-edge peaks suggests that metallic Cu fraction increases from about 60% of the pristine AgCu alloy, to about 90% after 40 min, and approaches 100% after 80 min of electroreduction (Figure 7a and S16). Corresponding extended X-ray absorption fine structure (EXAFS) spectra shows the diminution of Cu-O bonding and the increasing contributions of Cu-Cu bonding (Figure 7d and S17). These *operando* X-ray studies suggest that metallic Cu is the active state for catalyzing CO_2RR.

One pressing challenge facing the development of Cu electrocatalysts is whether the re-oxidation (*i.e.*, deactivation) of active metallic Cu sites (ref) can be mitigated or minimized, so as to maintain active structures after the CO_2RR and enhance the catalyst durability in realistic applications. After three-week air exposure, we examined the *ex-situ* XAS of AgCu electrocatalysts (Figure 7c and 7d). Surprisingly, the evolved AgCu catalysts exhibit a significant fraction of metallic Cu, as indicated by the horizontal dashes line in XANES spectra (Figure 7c). Examination of k^2-weighted EXAFS spectra clearly shows that AgCu electrocatalysts experience electroreduction from Cu_2O to metallic Cu during CO_2RR (red dashed arrows) (Figure 7d). Upon long-time air exposure, Cu in the evolved AgCu catalysts mainly maintains the metallic feature, as evidenced by the lack of Cu-O bonding at 1.5 Å and the persistent existence of triplet metallic Cu features at ~4.5 Å. The amplitude of Cu-Cu bonding exhibits a noticeable decay upon air exposure (green dashed arrows), which is possibly due to the structural reconstruction, such as fracturing of large Cu domains, leading to lower coordination numbers and/or more disordered structures upon air exposure. Collectively, *operando* HERFD XANES and EXAFS present unambiguous evidence to show that Cu in the AgCu catalysts is fully reduced to metallic Cu as possible active sites for the CO_2RR, and Ag in the evolved AgCu catalysts is instrumental in suppressing Cu oxidation upon air exposure.

In summary, we systematically explored the structural and chemical evolution of phase-blended and phase-separated AgCu catalysts under electrochemical CO_2RR conditions. Cu exhibits high mobility during CO_2RR, which can migrate to the catalyst surface, detach from the catalysts, and recrystallize as new particles. Meanwhile, the poor compatibility between Ag and Cu triggers their separation in spite of their initial mixing state. Eventually, the catalysts will evolve into structures composed of two phases, *i.e.*, $Ag_{0.88}Cu_{0.12}$ and $Ag_{0.05}Cu_{0.95}$, that are thermodynamically stable under CO_2RR conditions. This separation phenomenon not only occurs in the bulk of the catalysts, but also on the catalyst surface, suggesting that AgCu phase

heterostructures account for the enhanced CO_2RR in AgCu catalysts. In terms of the valence state, our *operando* XAS study confirms the Cu(0) state in the AgCu catalysts during the reaction, as well as the enhanced anti-oxidation of the evolved AgCu catalysts, as compared with Cu catalysts. Our work unveils how AgCu bimetallic catalysts structurally and chemically evolve during CO_2RR, which advances the understanding of the interaction between Cu and Ag, sheds light on the active AgCu structures for CO_2RR, and provides insights into the design of efficient AgCu catalysts for CO_2RR.

References

1. Bushuyev, O. S.; De Luna, P.; Dinh, C. T.; Tao, L.; Saur, G.; van de Lagemaat, J.; Kelley, S. O.; Sargent, E. H., What Should We Make with CO2 and How Can We Make It? *Joule* **2018,** *2* (5), 825-832.
2. Hepburn, C.; Adlen, E.; Beddington, J.; Carter, E. A.; Fuss, S.; Mac Dowell, N.; Minx, J. C.; Smith, P.; Williams, C. K., The technological and economic prospects for CO2 utilization and removal. *Nature* **2019,** *575* (7781), 87-97.
3. Ross, M. B.; De Luna, P.; Li, Y.; Dinh, C.-T.; Kim, D.; Yang, P.; Sargent, E. H., Designing materials for electrochemical carbon dioxide recycling. *Nat. Catal.* **2019,** *2* (8), 648-658.
4. Varela, A. S.; Ju, W.; Bagger, A.; Franco, P.; Rossmeisl, J.; Strasser, P., Electrochemical Reduction of CO2 on Metal-Nitrogen-Doped Carbon Catalysts. *ACS Catal.* **2019,** *9* (8), 7270-7284.
5. Birdja, Y. Y.; Pérez-Gallent, E.; Figueiredo, M. C.; Göttle, A. J.; Calle-Vallejo, F.; Koper, M. T. M., Advances and challenges in understanding the electrocatalytic conversion of carbon dioxide to fuels. *Nat. Energy* **2019,** *4* (9), 732-745.
6. Nitopi, S.; Bertheussen, E.; Scott, S. B.; Liu, X.; Engstfeld, A. K.; Horch, S.; Seger, B.; Stephens, I. E. L.; Chan, K.; Hahn, C.; Nørskov, J. K.; Jaramillo, T. F.; Chorkendorff, I., Progress and Perspectives of Electrochemical CO2 Reduction on Copper in Aqueous Electrolyte. *Chem. Rev.* **2019,** *119* (12), 7610-7672.
7. Lee, C. W.; Yang, K. D.; Nam, D.-H.; Jang, J. H.; Cho, N. H.; Im, S. W.; Nam, K. T., Defining a Materials Database for the Design of Copper Binary Alloy Catalysts for Electrochemical CO2 Conversion. *Adv. Mater.* **2018,** *30* (42), 1704717.
8. Bagger, A.; Ju, W.; Varela, A. S.; Strasser, P.; Rossmeisl, J., Electrochemical CO2 Reduction: A Classification Problem. *ChemPhysChem* **2017,** *18* (22), 3266-3273.
9. Liu, K.; Ma, M.; Wu, L.; Valenti, M.; Cardenas-Morcoso, D.; Hofmann, J. P.; Bisquert, J.; Gimenez, S.; Smith, W. A., Electronic Effects Determine the Selectivity of Planar Au–Cu Bimetallic Thin Films for Electrochemical CO2 Reduction. *ACS Appl. Mater. Inter.* **2019,** *11* (18), 16546-16555.
10. Nellaiappan, S.; Katiyar, N. K.; Kumar, R.; Parui, A.; Malviya, K. D.; Pradeep, K. G.; Singh, A. K.; Sharma, S.; Tiwary, C. S.; Biswas, K., High-Entropy Alloys as Catalysts for the CO2 and CO Reduction Reactions: Experimental Realization. *ACS Catal.* **2020,** *10* (6), 3658-3663.
11. Morales-Guio, C. G.; Cave, E. R.; Nitopi, S. A.; Feaster, J. T.; Wang, L.; Kuhl, K. P.; Jackson, A.; Johnson, N. C.; Abram, D. N.; Hatsukade, T.; Hahn, C.; Jaramillo, T. F., Improved CO2 reduction activity towards C2+ alcohols on a tandem gold on copper electrocatalyst. *Nat. Catal.* **2018,** *1* (10), 764-771.
12. Zhang, H.; Chang, X.; Chen, J. G.; Goddard, W. A.; Xu, B.; Cheng, M.-J.; Lu, Q., Computational and experimental demonstrations of one-pot tandem catalysis for electrochemical carbon dioxide reduction to methane. *Nat. Commun.* **2019,** *10* (1), 3340.
13. Kim, D.; Yu, S.; Zheng, F.; Roh, I.; Li, Y.; Louisia, S.; Qi, Z.; Somorjai, G. A.; Frei, H.; Wang, L.-W.; Yang, P., Selective CO2 electrocatalysis at the pseudocapacitive nanoparticle/ordered-ligand interlayer. *Nat. Energy* **2020,** *5* (12), 1032-1042.
14. Bui, J. C.; Kim, C.; King, A. J.; Romiluyi, O.; Kusoglu, A.; Weber, A. Z.; Bell, A. T., Engineering Catalyst–Electrolyte Microenvironments to Optimize the Activity and Selectivity for the Electrochemical Reduction of CO2 on Cu and Ag. *Acc. Chem. Res.* **2022,** *55* (4), 484-494.
15. Alloy Phase Diagrams. *ASM Handbook*; Okamoto, H., Schlesinger, M. E., Mueller, E. M., Eds.; ASM International: Materials Park, OH, 2016; Vol. 3.
16. Chen, P. C.; Liu, X. L.; Hedrick, J. L.; Xie, Z.; Wang, S. Z.; Lin, Q. Y.; Hersam, M. C.; Dravid, V. P.; Mirkin, C. A., Polyelemental nanoparticle libraries. *Science* **2016,** *352* (6293), 1565-1569.
17. Chen, P. C.; Du, J. S. S.; Meckes, B.; Huang, L. L.; Xie, Z.; Hedrick, J. L.; Dravid, V. P.; Mirkin, C. A., Structural Evolution of Three-Component Nanoparticles in Polymer Nanoreactors. *J. Am. Chem. Soc.* **2017,** *139* (29), 9876-9884.

18. Chen, P. C.; Liu, M. H.; Du, J. S. S.; Meckes, B.; Wang, S. Z.; Lin, H. X.; Dravid, V. P.; Wolverton, C.; Mirkin, C. A., Interface and heterostructure design in polyelemental nanoparticles. *Science* **2019,** *363* (6430), 959-964.
19. Chen, C.; Li, Y.; Yu, S.; Louisia, S.; Jin, J.; Li, M.; Ross, M. B.; Yang, P., Cu-Ag Tandem Catalysts for High-Rate CO2 Electrolysis toward Multicarbons. *Joule* **2020,** *4* (8), 1688-1699.
20. Gurudayal; Perone, D.; Malani, S.; Lum, Y.; Haussener, S.; Ager, J. W., Sequential Cascade Electrocatalytic Conversion of Carbon Dioxide to C–C Coupled Products. *ACS Appl. Energy Mater.* **2019,** *2* (6), 4551-4559.
21. Lum, Y.; Ager, J. W., Sequential catalysis controls selectivity in electrochemical CO2 reduction on Cu. *Energy Environ. Sci.* **2018,** *11* (10), 2935-2944.
22. Chen, C.; Yu, S.; Yang, Y.; Louisia, S.; Roh, I.; Jin, J.; Chen, S.; Chen, P.-C.; Shan, Y.; Yang, P., Exploration of the bio-analogous asymmetric C–C coupling mechanism in tandem CO2 electroreduction. *Nat. Catal.* **2022**, DOI: 10.1038/s41929-022-00844-w.
23. Dutta, A.; Montiel, I. Z.; Erni, R.; Kiran, K.; Rahaman, M.; Drnec, J.; Broekmann, P., Activation of bimetallic AgCu foam electrocatalysts for ethanol formation from CO2 by selective Cu oxidation/reduction. *Nano Energy* **2020,** *68*, 104331.
24. Huang, J.; Mensi, M.; Oveisi, E.; Mantella, V.; Buonsanti, R., Structural Sensitivities in Bimetallic Catalysts for Electrochemical CO2 Reduction Revealed by Ag–Cu Nanodimers. *J. Am. Chem. Soc.* **2019,** *141* (6), 2490-2499.
25. O'Mara, P. B.; Wilde, P.; Benedetti, T. M.; Andronescu, C.; Cheong, S.; Gooding, J. J.; Tilley, R. D.; Schuhmann, W., Cascade Reactions in Nanozymes: Spatially Separated Active Sites inside Ag-Core–Porous-Cu-Shell Nanoparticles for Multistep Carbon Dioxide Reduction to Higher Organic Molecules. *J. Am. Chem. Soc.* **2019,** *141* (36), 14093-14097.
26. Lee, S.; Park, G.; Lee, J., Importance of Ag–Cu Biphasic Boundaries for Selective Electrochemical Reduction of CO2 to Ethanol. *ACS Catal.* **2017,** *7* (12), 8594-8604.
27. Ting, L. R. L.; Piqué, O.; Lim, S. Y.; Tanhaei, M.; Calle-Vallejo, F.; Yeo, B. S., Enhancing CO2 Electroreduction to Ethanol on Copper–Silver Composites by Opening an Alternative Catalytic Pathway. *ACS Catal.* **2020,** *10* (7), 4059-4069.
28. Gao, J.; Zhang, H.; Guo, X.; Luo, J.; Zakeeruddin, S. M.; Ren, D.; Grätzel, M., Selective C–C Coupling in Carbon Dioxide Electroreduction via Efficient Spillover of Intermediates As Supported by Operando Raman Spectroscopy. *J. Am. Chem. Soc.* **2019,** *141* (47), 18704-18714.
29. Chen, P.-C.; Gao, M.; Yu, S.; Jin, J.; Song, C.; Salmeron, M.; Scott, M. C.; Yang, P., Revealing the Phase Separation Behavior of Thermodynamically Immiscible Elements in a Nanoparticle. *Nano Lett.* **2021,** *21* (15), 6684-6689.
30. Clark, E. L.; Hahn, C.; Jaramillo, T. F.; Bell, A. T., Electrochemical CO2 Reduction over Compressively Strained CuAg Surface Alloys with Enhanced Multi-Carbon Oxygenate Selectivity. *J. Am. Chem. Soc.* **2017,** *139* (44), 15848-15857.
31. Wang, X.; Wang, Z.; Zhuang, T.-T.; Dinh, C.-T.; Li, J.; Nam, D.-H.; Li, F.; Huang, C.-W.; Tan, C.-S.; Chen, Z.; Chi, M.; Gabardo, C. M.; Seifitokaldani, A.; Todorović, P.; Proppe, A.; Pang, Y.; Kirmani, A. R.; Wang, Y.; Ip, A. H.; Richter, L. J.; Scheffel, B.; Xu, A.; Lo, S.-C.; Kelley, S. O.; Sinton, D.; Sargent, E. H., Efficient upgrading of CO to C3 fuel using asymmetric C-C coupling active sites. *Nat. Commun.* **2019,** *10* (1), 5186.
32. Li, Y. C.; Wang, Z.; Yuan, T.; Nam, D.-H.; Luo, M.; Wicks, J.; Chen, B.; Li, J.; Li, F.; de Arquer, F. P. G.; Wang, Y.; Dinh, C.-T.; Voznyy, O.; Sinton, D.; Sargent, E. H., Binding Site Diversity Promotes CO2 Electroreduction to Ethanol. *J. Am. Chem. Soc.* **2019,** *141* (21), 8584-8591.
33. Hoang, T. T. H.; Verma, S.; Ma, S.; Fister, T. T.; Timoshenko, J.; Frenkel, A. I.; Kenis, P. J. A.; Gewirth, A. A., Nanoporous Copper–Silver Alloys by Additive-Controlled Electrodeposition for the Selective Electroreduction of CO2 to Ethylene and Ethanol. *J. Am. Chem. Soc.* **2018,** *140* (17), 5791-5797.

34. Chang, C.-J.; Lin, S.-C.; Chen, H.-C.; Wang, J.; Zheng, K. J.; Zhu, Y.; Chen, H. M., Dynamic Reoxidation/Reduction-Driven Atomic Interdiffusion for Highly Selective CO2 Reduction toward Methane. *J. Am. Chem. Soc.* **2020,** *142* (28), 12119-12132.
35. Yang, C.; Ko, B. H.; Hwang, S.; Liu, Z.; Yao, Y.; Luc, W.; Cui, M.; Malkani, A. S.; Li, T.; Wang, X.; Dai, J.; Xu, B.; Wang, G.; Su, D.; Jiao, F.; Hu, L., Overcoming immiscibility toward bimetallic catalyst library. *Sci. Adv.* **2020,** *6* (17), eaaz6844.
36. Chen, P.-C.; Li, M.; Jin, J.; Yu, S.; Chen, S.; Chen, C.; Salmeron, M.; Yang, P., Heterostructured Au–Ir Catalysts for Enhanced Oxygen Evolution Reaction. *ACS Mater. Lett.* **2021,** *3* (10), 1440-1447.
37. Wilde, P.; O'Mara, P. B.; Junqueira, J. R. C.; Tarnev, T.; Benedetti, T. M.; Andronescu, C.; Chen, Y.-T.; Tilley, R. D.; Schuhmann, W.; Gooding, J. J., Is Cu instability during the CO2 reduction reaction governed by the applied potential or the local CO concentration? *Chem. Sci.* **2021,** *12* (11), 4028-4033.
38. Huang, J.; Hörmann, N.; Oveisi, E.; Loiudice, A.; De Gregorio, G. L.; Andreussi, O.; Marzari, N.; Buonsanti, R., Potential-induced nanoclustering of metallic catalysts during electrochemical CO2 reduction. *Nat. Commun.* **2018,** *9* (1), 3117.
39. Wang, H.; Zhou, X.; Yu, T.; Lu, X.; Qian, L.; Liu, P.; Lei, P., Surface restructuring in AgCu single-atom alloy catalyst and self-enhanced selectivity toward CO2 reduction. *Electrochimica Acta* **2022,** *426*, 140774.
40. Fei, H.; Dong, J.; Wan, C.; Zhao, Z.; Xu, X.; Lin, Z.; Wang, Y.; Liu, H.; Zang, K.; Luo, J.; Zhao, S.; Hu, W.; Yan, W.; Shakir, I.; Huang, Y.; Duan, X., Microwave-Assisted Rapid Synthesis of Graphene-Supported Single Atomic Metals. *Adv. Mater.* **2018,** *30* (35), 1802146.
41. Popović, S.; Smiljanić, M.; Jovanovič, P.; Vavra, J.; Buonsanti, R.; Hodnik, N., Stability and Degradation Mechanisms of Copper-Based Catalysts for Electrochemical CO2 Reduction. *Angew. Chem. Int. Ed.* **2020,** *59* (35), 14736-14746.
42. Lee, S. H.; Lin, J. C.; Farmand, M.; Landers, A. T.; Feaster, J. T.; Avilés Acosta, J. E.; Beeman, J. W.; Ye, Y.; Yano, J.; Mehta, A.; Davis, R. C.; Jaramillo, T. F.; Hahn, C.; Drisdell, W. S., Oxidation State and Surface Reconstruction of Cu under CO2 Reduction Conditions from In Situ X-ray Characterization. *J. Am. Chem. Soc.* **2021,** *143* (2), 588-592.
43. Wang, H.; Liang, Z.; Tang, M.; Chen, G.; Li, Y.; Chen, W.; Lin, D.; Zhang, Z.; Zhou, G.; Li, J.; Lu, Z.; Chan, K.; Tan, T.; Cui, Y., Self-Selective Catalyst Synthesis for CO2 Reduction. *Joule* **2019,** *3* (8), 1927-1936.
44. Wang, Y.; Wang, Z.; Dinh, C.-T.; Li, J.; Ozden, A.; Golam Kibria, M.; Seifitokaldani, A.; Tan, C.-S.; Gabardo, C. M.; Luo, M.; Zhou, H.; Li, F.; Lum, Y.; McCallum, C.; Xu, Y.; Liu, M.; Proppe, A.; Johnston, A.; Todorovic, P.; Zhuang, T.-T.; Sinton, D.; Kelley, S. O.; Sargent, E. H., Catalyst synthesis under CO2 electroreduction favours faceting and promotes renewable fuels electrosynthesis. *Nat. Catal.* **2020,** *3* (2), 98-106.
45. Möller, T.; Scholten, F.; Thanh, T. N.; Sinev, I.; Timoshenko, J.; Wang, X.; Jovanov, Z.; Gliech, M.; Roldan Cuenya, B.; Varela, A. S.; Strasser, P., Electrocatalytic CO2 Reduction on CuOx Nanocubes: Tracking the Evolution of Chemical State, Geometric Structure, and Catalytic Selectivity using Operando Spectroscopy. *Angew. Chem. Int. Ed.* **2020,** *59* (41), 17974-17983.
46. Timoshenko, J.; Roldan Cuenya, B., In Situ/Operando Electrocatalyst Characterization by X-ray Absorption Spectroscopy. *Chem. Rev.* **2021,** *121* (2), 882-961.
47. Deng, Y.; Handoko, A. D.; Du, Y.; Xi, S.; Yeo, B. S., In Situ Raman Spectroscopy of Copper and Copper Oxide Surfaces during Electrochemical Oxygen Evolution Reaction: Identification of CuIII Oxides as Catalytically Active Species. *ACS Catal.* **2016,** *6* (4), 2473-2481.
48. Huang, X.; Zhao, Z.; Cao, L.; Chen, Y.; Zhu, E.; Lin, Z.; Li, M.; Yan, A.; Zettl, A.; Wang, Y. M.; Duan, X.; Mueller, T.; Huang, Y., High-performance transition metal–doped Pt₃Ni octahedra for oxygen reduction reaction. *Science* **2015,** *348* (6240), 1230-1234.

49. Arán-Ais, R. M.; Scholten, F.; Kunze, S.; Rizo, R.; Roldan Cuenya, B., The role of in situ generated morphological motifs and Cu(i) species in C2+ product selectivity during CO2 pulsed electroreduction. *Nat. Energy* **2020,** *5* (4), 317-325.
50. Li, Y.; Kim, D.; Louisia, S.; Xie, C.; Kong, Q.; Yu, S.; Lin, T.; Aloni, S.; Fakra, S. C.; Yang, P., Electrochemically scrambled nanocrystals are catalytically active for CO₂-to-multicarbons. *Proc. Nat. Acad. Sci. U.S.A.* **2020,** *117* (17), 9194-9201.
51. Sebastián-Pascual, P.; Escudero-Escribano, M., Surface characterization of copper electrocatalysts by lead underpotential deposition. *J. Electroanal. Chem.* **2021,** *896*, 115446.
52. Glatzel, P.; Bergmann, U., High resolution 1s core hole X-ray spectroscopy in 3d transition metal complexes—electronic and structural information. *Coord. Chem. Rev.* **2005,** *249* (1), 65-95.
53. Walroth, R. C.; Uebler, J. W. H.; Lancaster, K. M., Probing CuI in homogeneous catalysis using high-energy-resolution fluorescence-detected X-ray absorption spectroscopy. *Chem. Commun.* **2015,** *51* (48), 9864-9867.
54. Yang, Y.; Xiong, Y.; Zeng, R.; Lu, X.; Krumov, M.; Huang, X.; Xu, W.; Wang, H.; DiSalvo, F. J.; Brock, J. D.; Muller, D. A.; Abruña, H. D., Operando Methods in Electrocatalysis. *ACS Catal.* **2021,** *11* (3), 1136-1178.
55. Yang, Y.; Peltier, C. R.; Zeng, R.; Schimmenti, R.; Li, Q. *et al.*, Electrocatalysis in Alkaline Media and Alkaline Membrane-Based Energy Technologies. *Chem. Rev.* **2022,** *122* (6), 6117-6321.
56. Friebel, D.; Louie, M. W.; Bajdich, M.; Sanwald, K. E.; Cai, Y.; Wise, A. M.; Cheng, M.-J.; Sokaras, D.; Weng, T.-C.; Alonso-Mori, R.; Davis, R. C.; Bargar, J. R.; Nørskov, J. K.; Nilsson, A.; Bell, A. T., Identification of Highly Active Fe Sites in (Ni,Fe)OOH for Electrocatalytic Water Splitting. *J. Am. Chem. Soc.* **2015,** *137* (3), 1305-1313.
57. Yang, Y.; Wang, Y.; Xiong, Y.; Huang, X.; Shen, L.; Huang, R.; Wang, H.; Pastore, J. P.; Yu, S.-H.; Xiao, L.; Brock, J. D.; Zhuang, L.; Abruña, H. D., In Situ X-ray Absorption Spectroscopy of a Synergistic Co–Mn Oxide Catalyst for the Oxygen Reduction Reaction. *J. Am. Chem. Soc.* **2019,** *141* (4), 1463-1466.

Acknowledgments: This work is supported by…..

This work is based upon research conducted at the CHESS which is supported by the National Science Foundation under award DMR-1332208. We thank Dr. Christopher Pollock at CHESS PIPOXS beamlines for the HERFD XAS setup. P.-C.C. acknowledges support from Kavli ENSI Heising-Simons Fellowship. C.C and J.J. acknowledges fellowship support from Suzhou Industrial Park. Y.Y acknowledges support from Miller Fellowship. **Author contributions:** P.-C.C., C.C., and P.Y. conceived the ideas and designed the experiments. P.-C.C. and A.M. performed catalyst synthesis. P.-C.C. performed catalyst characterization. C.C. and J.F. conducted electrochemical tests. Y.Y. performed operando XAS measurements. J.J. discussed the experimental results. P.-C.C., C.C., Y.Y., and P.Y. wrote the manuscript with editorial input from the other authors. P.Y. supervised the project. **Competing interests:** The Authors declare no competing financial interests.

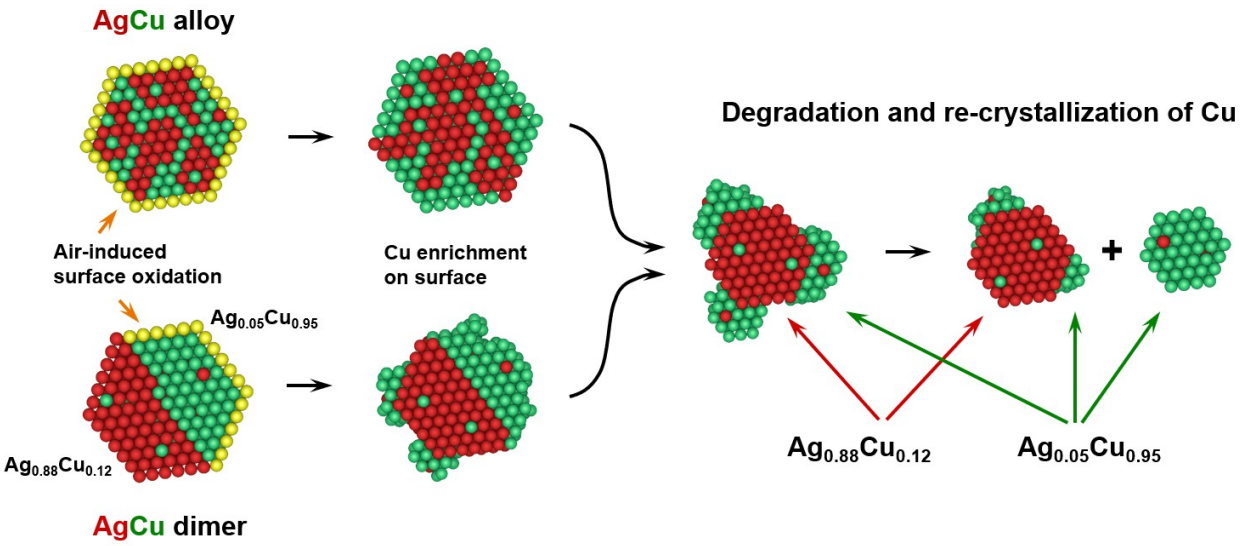

Fig. 1. Schematic illustration of the chemical and structural evolution of alloyed and phase-separated AgCu catalysts in electrochemical CO_2RR.

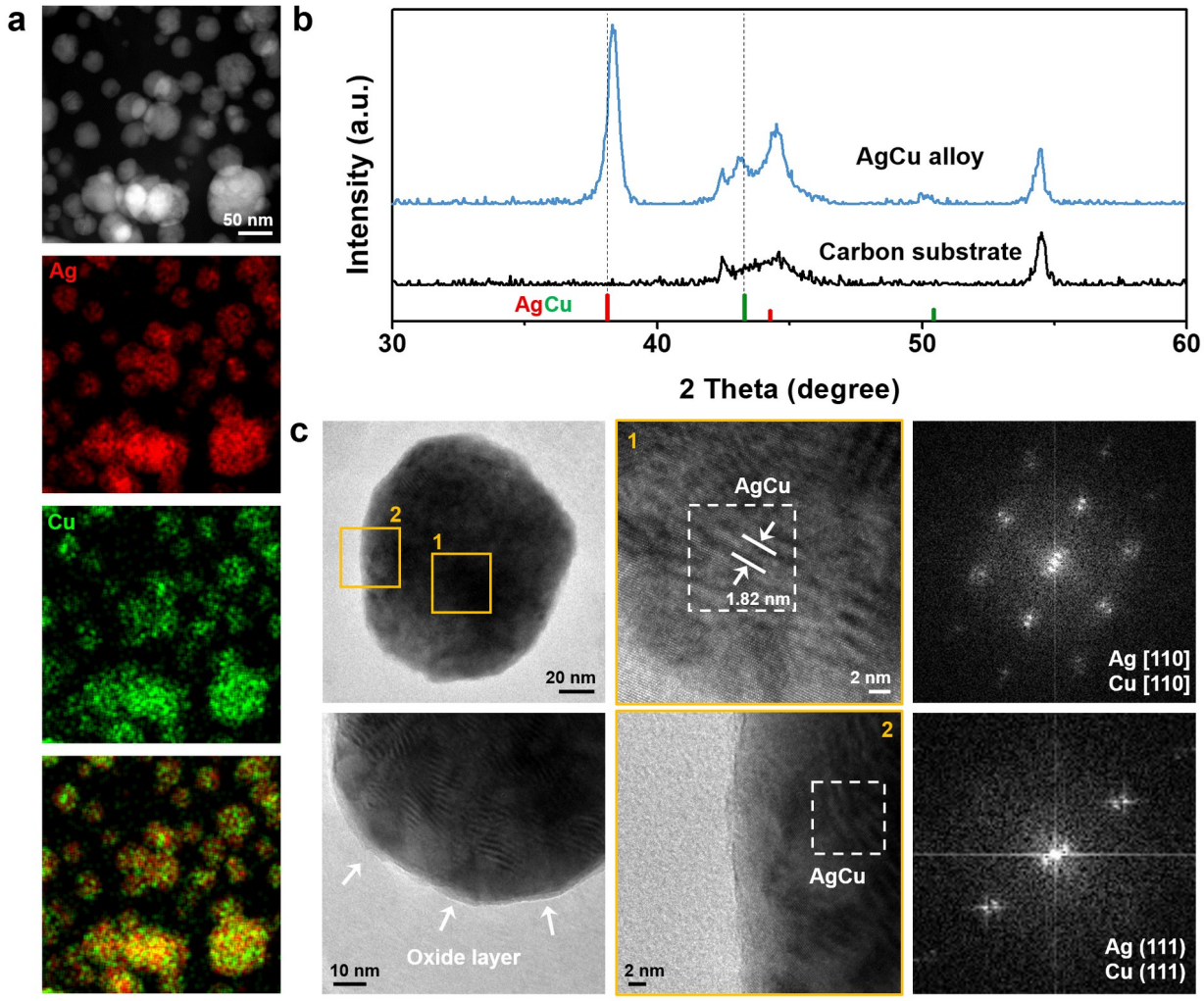

Fig. 2. Structural characterization of AgCu alloy catalysts made by microwave-assisted shock synthesis. (a) HAADF-STEM image and EDS elemental mapping of $Ag_{0.5}Cu_{0.5}$ alloy particles synthesized on carbon paper substrates. (b) XRD patterns of the carbon paper substrates and the as-synthesized AgCu alloy particles. (c) HRTEM characterization of the AgCu alloy particles. The orange squares in the first image denote the zoomed-in regions for imaging, which are shown in the second column. The white dash squares in the second column of images indicate the areas selected for FFT. The FFT results are shown in the third column.

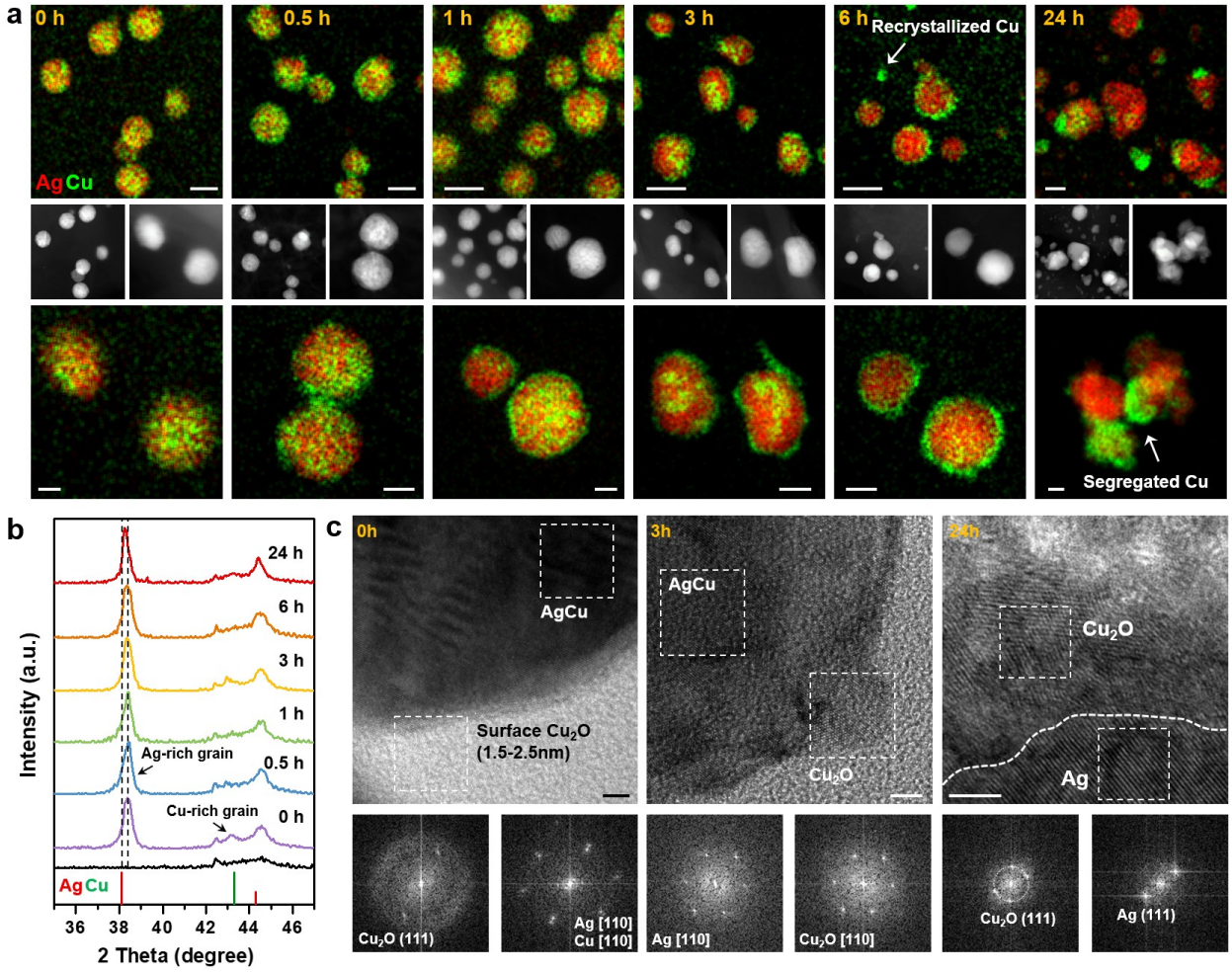

Fig. 3. Structural evolution of AgCu alloy catalysts in CO_2RR. (a) HAADF-STEM images and EDS elemental mapping of AgCu alloy catalysts after being used for 0 h, 0.5 h, 1 h, 3 h, 6 h, and 24 h of CO_2RR. Scale bars in the top row, 50 nm. Scale bars in the bottom row, 20 nm. (b) XRD patterns of AgCu alloy particles after catalyzing CO_2RR for a specific time. The black line is the XRD curve of carbon substrates. (c) HRTEM images of AgCu alloy catalysts after being used for 0 h, 3 h, and 24 h of CO_2RR. White dash squares highlight the regions used for FFT analysis. Scale bars, 3 nm.

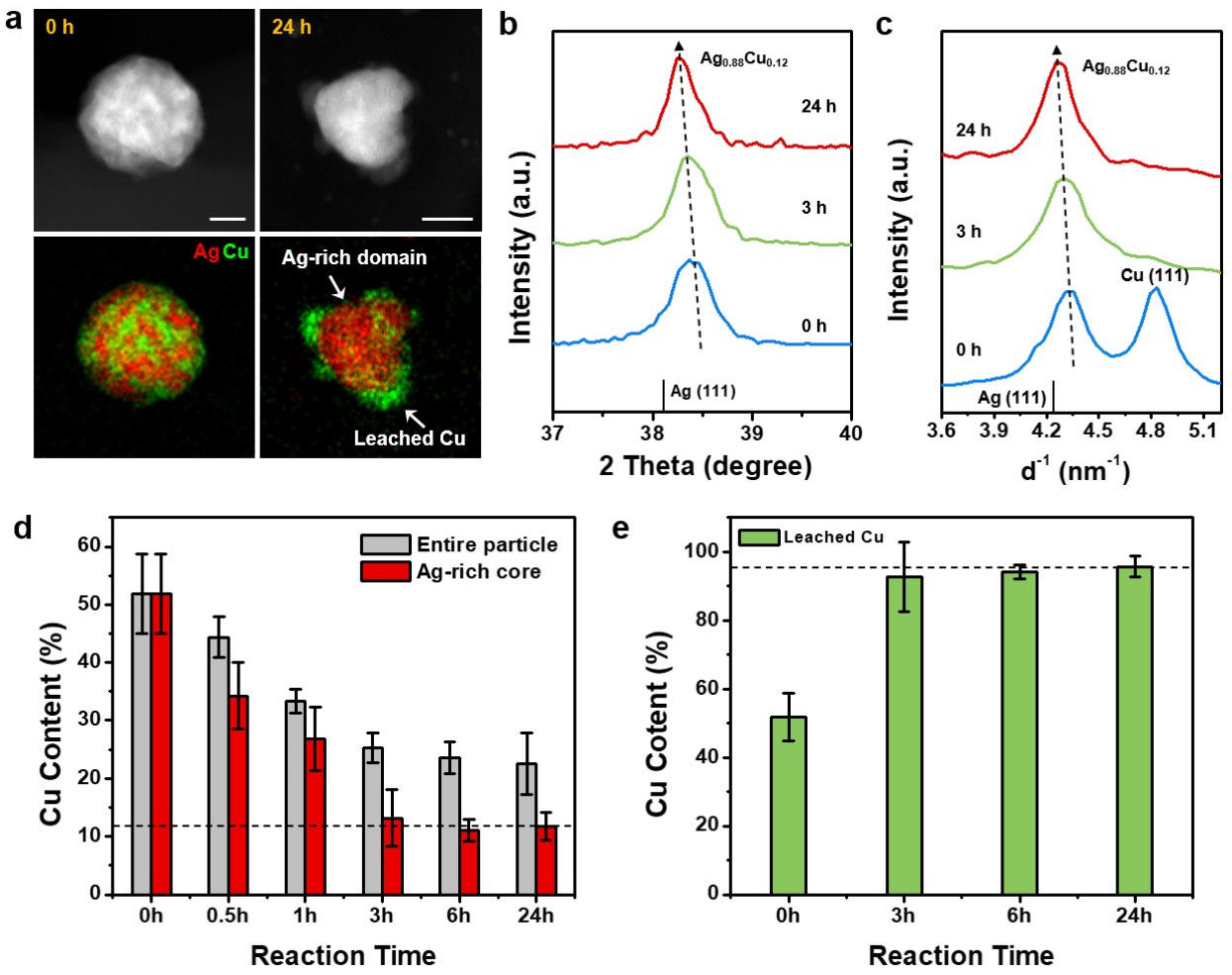

Fig. 4. Compositional evolution of AgCu alloy catalysts in CO_2RR. (a) HAADF-STEM images and EDS elemental mapping of an as-synthesized AgCu alloy particle and a particle after catalyzing CO_2RR for 24 h. Scale bars, 20 nm. (b) XRD patterns showing the change in the d-spacing of catalyst (111) planes during CO_2RR. (c) SAED radial intensity profiles of the regions near (111) diffraction, which show the change in the d-spacing of catalyst (111) planes during CO_2RR. (d) Compositional variation of the entire AgCu particles and the Ag-containing core of the catalysts during CO_2RR. (e) Compositional change of the leached Cu species during CO_2RR.

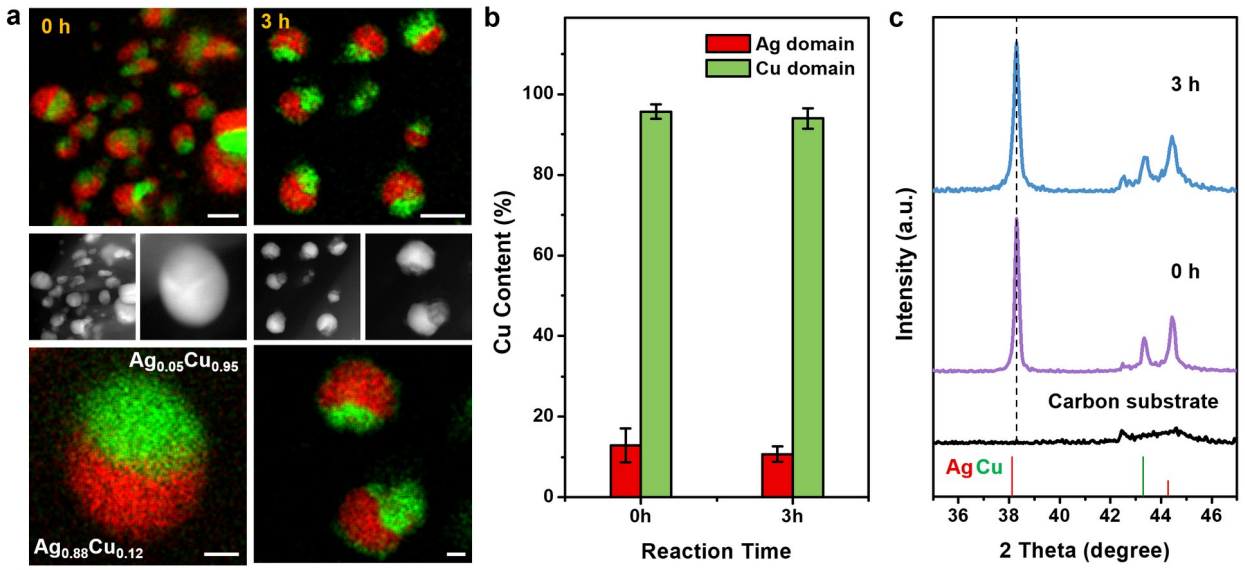

Fig. 5. Compositional evolution of phase-separated AgCu catalysts in CO_2RR. (a) HAADF-STEM images and EDS elemental mapping of as-synthesized phase-separated AgCu particles and particles after catalyzing CO_2RR for 3 h. Scale bars in the top row, 50 nm. Scale bars in the bottom row, 10 nm. (b) Compositional change of the Ag and Cu domains in the phase-separated AgCu catalysts during CO_2RR. (c) XRD patterns of the phase-separated AgCu catalysts and the catalysts used for 3 h of CO_2RR.

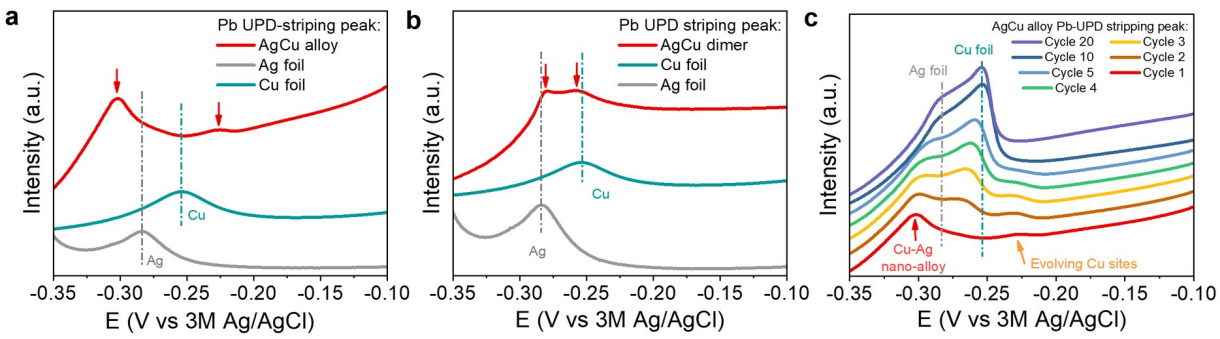

Fig. 6. Pd-UPD analysis of alloyed and phase-separated AgCu catalysts. (a) Pb stripping peaks of the AgCu alloy particles in Pb-UPD experiments. The first cycle was plotted here to avoid any surface reconstruction of the AgCu nanoalloy. Pb stripping peaks of Cu and Ag foils were included for comparison. (b) Pb stripping peaks of the phase-separated AgCu particles in Pb-UPD experiments. The first cycle was plotted here to avoid any surface reconstruction of the AgCu heterodimers. Pb stripping peaks of Cu and Ag foils were included for comparison. (c) Sequential Pb stripping peaks of the AgCu nanoalloy in Pb-UPD experiments. In the Pb-UPD experiments, Pb was deposited on AgCu nanoalloy during the cathodic scan and stripped in the anodic scan. 20 cyclic voltammetry cycles were recorded to track the surface evolution of the AgCu nanoalloy.

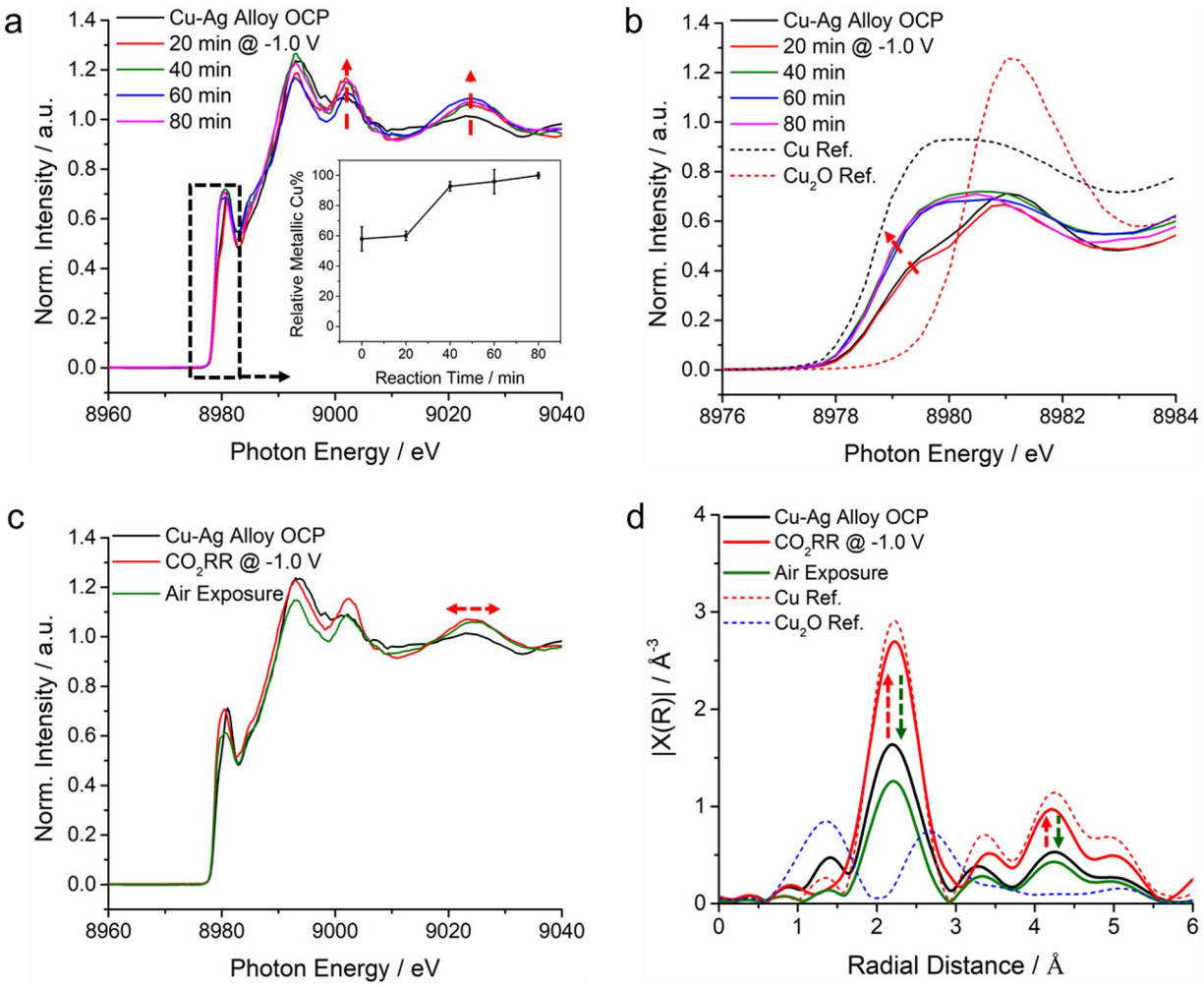

Fig. 7. *Operando* HERFD XAS studies of valence states and coordination environments of AgCu alloy catalysts. (a) *Operando* HERFD XANES of Cu K-edge of the AgCu alloy as a function of reaction time at -1.0 V vs. RHE in CO_2-sat. 0.1 M $KHCO_3$. Inset shows the quantitative analysis of relative metallic Cu fraction. (b) XANES pre-edges of AgCu alloy magnified from the dashed box region in (a) and the comparison with Cu and Cu_2O references (dashed lines). (c-d) *Operando* XANES and corresponding EXAFS spectra of AgCu before, during, and upon air exposure after the CO_2RR.